

https://dspace.org/

Seasonal Harvesting Impact on Biomass Fuel Properties and PyrolysisDerived BioOil Organic Phase Composition

M Shezi; S.L Kiambi; Yusuf Isa

WILEY-BLACKWELL
https://hdl.handle.net/10539/43441
WOS

Downloaded from a DSpace repository. https://dspace.org/

Check for updates

GCB Bioenergy

WILEY

Global Change Biology Bioenergy
BIOPRODUCTS FOR A SUSTAINABLE BIOECONOMY

RESEARCH ARTICLE OPEN ACCESS

Seasonal Harvesting Impact on Biomass Fuel Properties and Pyrolysis-Derived Bio-Oil Organic Phase Composition

Manqoba Shezi[1] | Sammy Lewis Kiambi[2] | Yusuf Makarfi Isa[3]

[1]Durban University of Technology, Durban, South Africa | [2]Chemical Engineering Department, Vaal University of Technology, Vanderbilpark, South Africa | [3]School of Chemical and Metallurgical Engineering, University of the Witwatersrand, Johannesburg, South Africa

Correspondence: Manqoba Shezi (manqoba.shezi@fulbrightmail.org)

Received: 8 September 2024 | **Revised:** 30 October 2024 | **Accepted:** 1 November 2024

Funding: This work was supported by National Research Foundation (NRF) and Durban University of Technology.

Keywords: biochar | biofuels | biomass | bio-oil | fast pyrolysis | Giant Reed | harvest seasons | invasive species

ABSTRACT

Thermochemical conversion of giant reed biomass during periodic variations has been carried out in a semi-batch tubular reactor at 550°C. This study was carried out after the incineration of giant reed along the river banks. Four periodic variations, late spring (HS-4), late summer (HS-1), late autumn (HS-2), and late winter (HS-3) were considered to investigate the effect of harvest time on biomass fuel properties, pyrolysis product distribution, non-condensable gas characterization, and bio-oil organic phase (BOP) fuel properties. The considered biomasses herein had average calorific values of 18.86 ± 0.05, 19.73 ± 0.05, 19.23 ± 0.04, and 18.44 ± 0.04 MJ/kg during HS-1, HS-2, HS-3, and HS-4, respectively. The biomass, bio-oil organic phase, biochar, and pyrolysis gas were characterized using thermogravimetric analysis (TGA), gas chromatography–mass spectroscopy (GCMS), Fourier transform infrared spectroscopy (FTIR), micro-GC, and scanning electron microscopy (SEM/EDS). The organic phase of bio-oil was isolated using a 125 mL separating funnel, allowing natural stratification of the immiscible phases. BOP yield increased from 5 to 11 wt% during HS-4 and HS-3, respectively. Higher heating values (HHV) of the BOP ranged from 19.4 ± 0.03 to 22.6 ± 0.02 MJ/kg in relation to the active growth stage and senescence-dormant phase. Physical and chemical properties (TAN, density, viscosity, water content, and CHNS) and chemical compound groups of organic phase bio-oil were analyzed. The produced BOP was rich in phenolics for all considered periods. The effect of harvest time showed that biomass and bio-oil organic phase fuel properties are improved during the senescence-dormant period. As a result, giant reed biomass should be harvested during autumn to avoid incineration that releases carbon dioxide into the atmosphere and will also reduce the occurrence of artificial flooding.

1 | Introduction

The continued use of fossil fuels poses a severe challenge because of the world's limited supply, energy insecurity, and environmental concerns over global warming due to the production of greenhouse gases (Fernandez et al. 2021; Patel, Agrawal, and Rawal 2020). Inevitably, the world will run out of oil that can be mined and burned in the long term. Sustainable energy transport and infrastructure are the endpoints. Dependence on fossil fuels is dangerous and poses a significant threat to biodiversity; thus, attaining sustainable energy transport and infrastructure is critical. Additionally, dependence on fossil fuels for energy has tampered with the natural carbon cycle. It is well known that the natural carbon cycle has existed for millions of years, and there was no urgency around it. The problem started when extra carbon was added to the natural carbon cycle through human activities, and the net result is that the carbon in the atmosphere is increasing over time. It is much more than that can be absorbed by the ecosystem. As a result, it has become evident

This is an open access article under the terms of the Creative Commons Attribution License, which permits use, distribution and reproduction in any medium, provided the original work is properly cited.

© 2024 The Author(s). *GCB Bioenergy* published by John Wiley & Sons Ltd.

that energy should be renewable, cost-effective, convenient, safe, and sustainable. Nowadays, it is considered feasible and promising to convert biomass via thermochemical processes into petrochemicals and biofuels (Çağlar and Demirbaş 2002). These processes use various biomasses that can be processed into a wide range of products, offering great productivity. In thermochemical conversion, the primary techniques include pyrolysis, liquefaction, gasification, and combustion (Awasthi et al. 2023). Among the aforementioned thermochemical techniques, pyrolysis is the preferred approach, as it is cost-effective and easy to use to produce biofuels and petrochemicals from biomass. This technique is categorized into slow, fast, and flash pyrolysis (Pawar, Panwar, and Salvi 2020). The choice of pyrolysis type to use depends on the desired product distribution.

Fast pyrolysis is a good choice when high bio-oil yields are desired, while slow and flash are selective to higher yields of biochar and pyrolysis gas, respectively. The bio-oil from fast pyrolysis is a potential source of valuable petrochemicals; however, due to undesired properties, it is incompatible with direct application as an engine fuel (Lohitharn and Shanks 2009). Low heating value and high water content, acidity, and corrosiveness are well-known limitations of raw bio-oil. The aforementioned drawbacks of raw bio-oil are attributed to the presence of oxygenated compounds such as phenols, alcohols, furans, water, acids, ketones, and aldehydes (Auersvald et al. 2019; Oasmaa, Kuoppala, and Elliott 2012). Giant reed species make it to the top 100 most invasive plant species globally, as stated by the International Union for the Conservation of Nature (Lowe et al. 2000). This plant species has been allowed to grow without definitive and sustainable control in many parts of the world. Giant reed is well suited to subtropical and warm temperate regions and has been found in the Mediterranean basin for thousands of years (Ba et al. 2020; Saikia et al. 2015).

The significance of giant reed is justified as a non-food crop not only because of its high biomass yields, low agronomic input, and low production costs but also because of its versatility. Currently, there is no effective control measure for dealing with the extensive amount of invasive Giant reed. Incinerating it directly is the adopted technique to dispose of it; however, this releases harmful gases, which are carbon monoxide, carbon dioxide, nitrogen oxides, and fine particulate matter (Corno, Pilu, and Adani 2014). South Africa is no exception for not being able to deal with the invasive nature of giant reed. Artificial flooding was witnessed in Ladysmith (a semi-rural area in South Africa) in February 2021, which had a significant impact as it led to damage of property, loss of jobs, loss of shelter, and loss of cattle, among other impacts. The concentration of giant reed is high in Ladysmith (in riverbanks and in-land). During the flood, the stems and rhizomes of giant reed deposit in the drainage systems and under bridges, resulting in the blocking of waterways, structural damage, and hazards to bridges and other structures (Ba et al. 2020).

The attempts to apply biological and burning methodologies to control the invasiveness of the non-food plant add no value compared to utilizing the plant for bioenergy generation. Patel and Kumar (2016), investigated the pyrolysis of gigantic reed grass using TG-MS. The authors concluded that energy grass has a stronger thermochemical reactivity and a quicker devolatilization. Giant Reed has the potential to be a sustainable biorefinery feedstock due to its fast growth rate composition and is available year-round. The current study will look at pyrolyzing Giant Reed and characterizing the products. Furthermore, to the best of the author's knowledge, there is no study available in the literature on how the fuel properties of giant reed vary based on different harvest seasons after incineration from the previous year. This study aimed to investigate the effect of periodic variations on the fuel properties of giant reed and assess its influence on pyrolysis product yield, quality, and distribution.

2 | Materials And Methods

2.1 | Sample Harvesting and Preparation

The giant reed (*Arundo donax*) was harvested from the banks of Klip River in Ladysmith, Kwa-Zulu Natal, South Africa (28.5631°S, 29.7810°E). The harvesting was done in four different seasons, namely late spring (October), late summer (January), late autumn (April), and late winter (July) denoting HS-4, HS-1, HS-2, and HS-3, respectively. HS-4 and HS-1 were aligned with the active growth stage, whereas HS-2 and HS-3 were aligned with the senescence-dormant phase. Giant reed height from the ground was 2–6 m. The culm of the *A. donax* was considered in the current study. The culm was cut into pieces and then dried for 24 h at 105°C. The oven-dried biomass was ground by a micro plant grinder, followed by sieving to a particle size range of 0.5–2 mm.

2.2 | Estimation of Biomass Structural Composition

2.2.1 | Acid Insoluble Lignin

The Klason lignin was estimated by following the NREL method (Sluiter et al. 2008, 2005). Briefly, 10 g of biomass was loaded into the extraction crucible for a sequential water and ethanol extraction process. After extraction, 0.3 g of biomass was loaded into pressure tubes to conduct acid hydrolysis using 72% sulfuric acid. After the acid hydrolysis, Klason lignin (KL) was determined through filtration and oxidation.

2.2.2 | Detergent Fiber Method

Van Soest method (Van Soest, Robertson, and Lewis 1991) was adopted to estimate the quantities of cellulose, hemicellulose, and lignin. The technique involves the determination of acid detergent fiber (ADF), acid detergent lignin (ADL), and neutral detergent fiber (NDF) as follows:

To determine acid detergent fiber (ADF), 1 g of dried biomass and 100 mL of an acid detergent solution containing cetyltrimethylammonium bromide (CTAB) and 0.5 M H_2SO_4 were added

17571707, 2024, 12, Downloaded from https://onlinelibrary.wiley.com/doi/10.1111/gcbb.70011 by South African Medical Research, Wiley Online Library on [28/11/2024]. See the Terms and Conditions (https://onlinelibrary.wiley.com/terms-and-conditions) on Wiley Online Library for rules of use; OA articles are governed by the applicable Creative Commons License

to a flat bottom flask. After the mixture began to boil, it was refluxed for 1 h. The residue was washed with hot distilled water and acetone and then dried at 105°C ± 5°C until its weight remained constant.

$$\%\,\mathrm{ADF} = \frac{m_{C+ADF} - m_C}{m_{bm}} \times 100 \quad (1)$$

Acid detergent lignin (ADL) was determined by digesting ADF with 72% H_2SO_4 for 3 h. Digested ADF was then washed with hot deionized water through a filtering crucible. The residue was dried at 105°C ± 5°C until constant weight was achieved, followed by oxidation at 550°C for 5 h.

$$\%\,\mathrm{ADL} = \frac{m_{C+ADL} - m_C}{m_{bm}} \times 100 \quad (2)$$

The ash content was determined from the residue after 5 h oxidation at 550°C.

$$\%\,\mathrm{ASH} = \frac{m_{C+ASH} - m_C}{m_{bm}} \times 100 \quad (3)$$

Ethylene diamine tetra acetate acid and sodium dodecyl sulfate were used to prepare neutral detergent solutions (NDF). After the mixture began to boil, it was refluxed for 1 h. The residue was subjected to sequential rinsing, starting with hot deionized water followed by acetone, and then dried at 105°C ± 5°C until its weight remained constant.

$$\%\,\mathrm{NDF} = \frac{m_{C+NDF} - m_C}{m_{bm}} \times 100 \quad (4)$$

Based on NDF, ADF, and ADL, the contents of cellulose, hemicellulose, and lignin were computed as follows:

$$\mathrm{Hemicellulose} = \mathrm{NDF} - \mathrm{ADF} \quad (5)$$

$$\mathrm{Cellulose} = \mathrm{ADF} - \mathrm{ADL} \quad (6)$$

$$\mathrm{Lignin} = \mathrm{ADL} - \mathrm{Ash} \quad (7)$$

$$\mathrm{Others} = 100 - \mathrm{NDF} \quad (8)$$

Others include extractives, proteins, and lipids.

2.3 | Analytical Methods

Elemental analysis (CHNS) was performed using an Elementar Vario Micro Select, according to ASTM D5373 and ASTM D5291. The oxygen content was determined by difference, and the results were reported on a dry basis. The moisture content of bio-oil was measured by the Karl Fischer Titration method. Total acid number (TAN) was measured by a Mettler T50 auto titrator using a total acid number titration solvent mixture and 0.1 M KOH 2-propanol as the titrating reagent (titrant), according to ASTM D664-07. The viscosity (kinetic and dynamic) and density were measured using the Anton Paar Instrument (SVM Standard method) at 40°C. Biomass moisture and ash content were determined according to ASTM D4442-07 and E 1755–01, respectively. The volatiles were determined according to ASTM E872, and fixed carbon content was determined by difference.

A bomb calorimeter was used to determine the higher heating values of biomass and bio-oil organic phase. SEM/EDS was used to determine the contents of silicates and potassium on the internal and external surfaces of biomass. A muffle furnace was used during the oxidation processes. The thermal degradation behavior of biomass was carried out using a Thermogravimetric analyzer (TGA5500) under the nitrogen atmosphere for a temperature range of 25°C–800°C at a heating rate of 10°C/min. Platinum HT pan types were used for sample loading, and a ramp procedure was used. The data on weight loss of biomass as a function of temperature was used to interpret thermochemical decomposition behavior. The chemical functional groups of biomass and organic phase bio-oil were identified using a Fourier Transform Infrared spectroscopy (FTIR) at a range of 4000–400 cm^{-1}. The spectra were generated using the FTIR-ATR, Thermo Fisher Scientific Smart ITX (Nicolet iSO10) spectrometer. Pyrolysis gas chemical composition was analyzed using Agilent 490 4-channel Micro GC, with helium and argon as carrier gases for different channels. The calibration curves were initiated using a standard gas mixture of hydrogen (H_2), nitrogen (N_2), carbon monoxide (CO), carbon dioxide (CO_2), oxygen (O_2), ethene (C_2H_4), ethane (C_2H_6), and methane (CH_4). The "others (C_xH_y)" on the pyrolysis gas balance was obtained by difference, that is, non-quantified gases were classified as others. The chemical composition of organic phase bio-oil was analyzed by gas chromatography coupled with a mass spectrometric detector (GCMS). The experiments were carried out on an Agilent 5977C GC/MSD with helium gas as a carrier gas. National Institute of Standards and Technology (NIST) spectral library was used to identify the chemical compounds. The samples were weighed and then diluted with 2 mL of methanol. The diluted sample was injected, and the inlet temperature was set to 280°C at a split ratio of 10:1. The column temperature was held at 50°C for 5 min, then heated to 280°C at a ramping rate of 10°C/min with a 5 min holding time.

2.4 | Semi-Batch Pyrolysis Setup and Procedure

Pyrolysis experiments were performed in a 1.5 L stainless steel fixed bed reactor (FBR)—the representation of the pyrolysis system is shown in Figure 1. For a typical experimental run, 60 g of physically pretreated biomass was loaded into the reactor, followed by purging with nitrogen at 2 L/min to remove unwanted oxygen in the pyrolysis system. The nitrogen flow rate during the reaction was maintained at 2 L/min to maintain an inert atmosphere. A 3 kW electrical heater equipped with a temperature control panel was used as a heat source during the pyrolysis reaction. The furnace was heated from room temperature to the desired setpoint temperature of 550°C at a heating rate of 5°C/min. Condensable vapors from the pyrolysis reactor were cooled in a two-series condensing system using cold water as a cooling medium. The cooling water was continuously circulated at 5 L/min using a submersible pump. Ice cubes were added to

17571707, 2024, 12, Downloaded from https://onlinelibrary.wiley.com/doi/10.1111/gcbb.70001 by South African Medical Research, Wiley Online Library on [28/11/2024]. See the Terms and Conditions (https://onlinelibrary.wiley.com/terms-and-conditions) on Wiley Online Library for rules of use; OA articles are governed by the applicable Creative Commons License

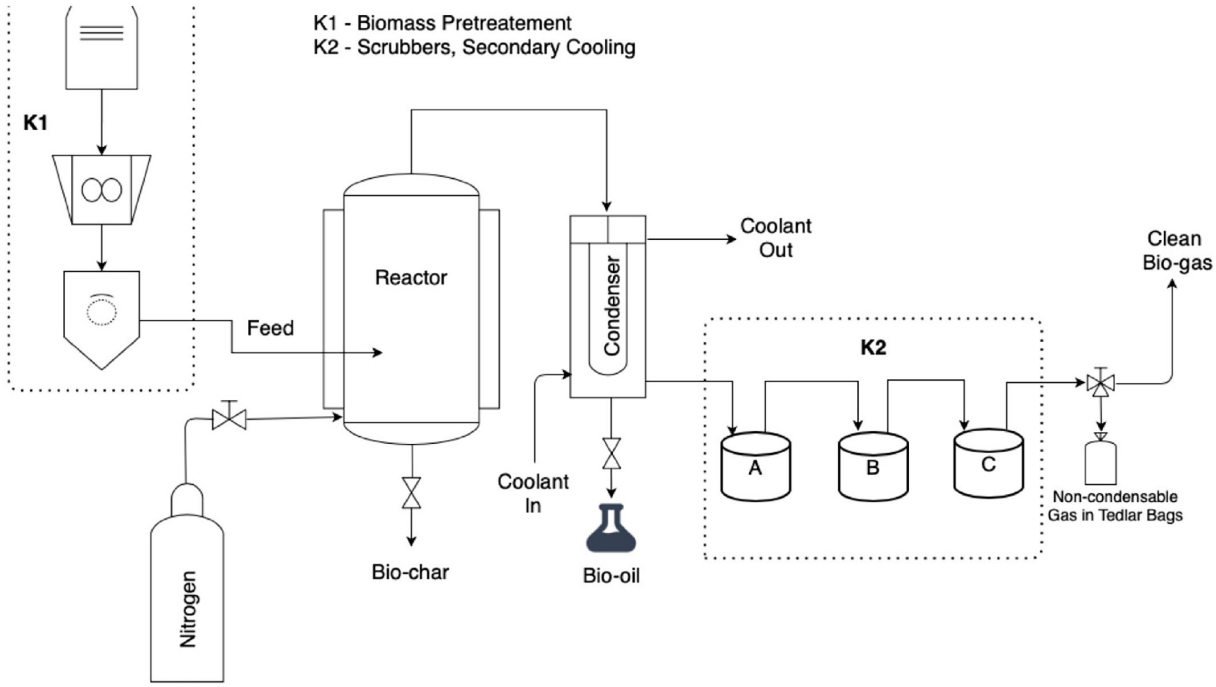


FIGURE 1 | Schematic representation of the semi-batch fast pyrolysis unit. The pyrolysis experiments were conducted in a 1.5 L stainless steel fixed-bed reactor (FBR). A 3-kW electrical heater with a temperature control panel was the heat source.

the circulating water to maintain the temperature at 5°C. The bio-oil was collected in two product bottles connected in series. Non-condensable gases were collected in 0.5 L Tedlar bags (CEL Scientific) 15 min after the pyrolysis reaction for compositional analyses was started. The pyrolysis reaction was allowed to run until no gas was coming out of the exhaust line, with an average reaction time of 45 ± 5 min per run. At the end of each experiment, the reactor was allowed to cool down to room temperature, and the reactor with biochar was weighed. The percentage yields of the bio-oil organic phase (BOP%), aqueous phase (BAP%), biochar (BC%), and pyrolysis gas (BG%) were calculated by the following equations:

$$\mathrm{BOP}\,\% = \frac{m_{bop}}{m_{bm}} \times 100 \tag{9}$$

$$\mathrm{BAP}\,\% = \frac{m_{bap}}{m_{bm}} \times 100 \tag{10}$$

$$\mathrm{BC}\,\% = \frac{m_{bc}}{m_{bm}} \times 100 \tag{11}$$

where m_{bop}, m_{bm}, m_{bap}, and m_{bc} are the masses of the organic phase, biomass, aqueous phase, and biochar, respectively. The principle of mass conservation was used to determine the pyrolysis gas production yield according to the following equation:

$$\mathrm{BG}\,\% = 100 - \mathrm{BC}\,\% - (\mathrm{BOP}\,\% + \mathrm{BAP}\,\%) \tag{12}$$

Energy density and distribution were determined for the bio-oil organic phase after the thermochemical conversion of biomass via fast pyrolysis, where X_P, HHV_P, and HHV_B are the product yield and heating values of product and biomass, respectively.

$$\text{Energy Density} = X_P HHV_P (1 - M_C) \tag{13}$$

$$\%\,\text{Energy Distribution} = \frac{HHV_P}{HHV_B} \times 100 \tag{14}$$

2.5 | Bio-Oil Phase Separation

This study used a conventional separation technique to isolate the aqueous (BAP) and organic (BOP) phases of bio-oil for quantification and analysis. Given their immiscibility, the two phases naturally stratified, with the aqueous phase on top and the denser organic phase settling at the bottom. A 125 mL separating funnel (conical and graduated with PTFE stopcock) separated the two immiscible phases. The organic phase, being heavier, was collected by carefully opening the stopcock at the bottom of the funnel until all of the phase was transferred into a flask, after which the stopcock was closed. Weights were measured to determine the yields of each phase, with the organic phase subjected to further analysis in accordance with the study's objectives. Numerous researchers have performed exceptional work in using solvent extraction methods for phase separation (Ahmed and Kishore 2023a, 2023b, 2024; Aravind, Ahmed, and Kishore 2023; Das and Goud 2021; David and Kopac 2018; Park et al. 2016). However, this research specifically aimed to retain the original properties of the BOP, thus avoiding solvent use. Moreover, many studies focusing on solvent extraction prioritize improving the BOP properties, which was different from the objective of this work; therefore, only conventional separation was deemed necessary. The aqueous phase primarily contained water-soluble compounds, whereas the organic phase was predominantly rich in water-insoluble phenolics, highlighting the distinct chemical compositions of the two fractions.

17571707, 2024, 12, Downloaded from https://onlinelibrary.wiley.com/doi/10.1111/gcbb.70011 by South African Medical Research, Wiley Online Library on [28/11/2024]. See the Terms and Conditions (https://onlinelibrary.wiley.com/terms-and-conditions) on Wiley Online Library for rules of use; OA articles are governed by the applicable Creative Commons License

3 | Results

3.1 | Composition of Biomass

The quality of the fuel is highly dependent on the raw material used. Hence, it is crucial to select feedstock with excellent fuel characteristics that are suitable for generating bioenergy. Fuel query parameters, such as ash content, fixed carbon, calorific value, and volatile matter content, will determine the fuel's operational attributes and performance.

The elemental composition analysis indicated variations in biomass characteristics over different seasons, as tabulated in Table 1. Carbon, a primary component, demonstrates marginal fluctuations across seasons, with the highest concentration observed during HS-2 at 49.69 ± 0.16 wt% and the lowest in HS-4 at 48.20 ± 0.13 wt%. Hydrogen content, essential for energy yield, exhibits analogous trends, peaking in HS-1 at 6.54 ± 0.16 wt% and decreasing in HS-3 to 6.30 ± 0.18 wt%. Nitrogen exhibits minor variability and exhibits heightened levels in HS-2 at 0.29 ± 0.03 wt%. Sulfur content, pertinent for fuel quality, notably varies, with HS-2 showing the highest concentration at 0.039 ± 0.01 wt%. Oxygen, pivotal for combustion characteristics, showcases fluctuations, with the highest levels recorded in HS-4 at 45.00 ± 0.23 wt%. C/H and H/C ratios also remain relatively constant, indicating consistent C-H relationships.

Conversely, the O/C ratio demonstrates slight variability, with the highest values in HS-4 at 0.93 ± 0.51 wt%. Furthermore, higher heating value (HHV) displays seasonal fluctuations, reaching a high in HS-2 at 19.73 ± 0.05 MJ/kg and decreasing in HS-4 to 18.44 ± 0.04 MJ/kg. The variations in heating values were mainly attributed to the high and low oxygen content in HS-4 and HS-2, respectively.

The volatile content of biomass increased from 85.8 ± 0.58 to 87.2 ± 0.61 wt% during HS-4 and HS-3, respectively, as seen in Table 2. Meanwhile, the moisture content decreased from 6.21 ± 0.14 to 4.32 ± 0.14 wt%. The volatile content is 86.8 ± 0.70 wt% in HS-2, slightly increasing compared to the HS-1 season (86.5 ± 0.73 wt%).

The ash content data in Table 2 shows significant variations across the different seasonal variations (HS-1 to HS-4). In HS-1, the ash content is 5.69 ± 0.04 wt%, whereas in HS-2, it decreases substantially to 2.01 ± 0.02 wt%. Similarly, in HS-3, the ash content further reduces to 1.95 ± 0.02 wt%, followed by a notable increase in HS-4 to 6.1 ± 0.03 wt%. The spectrum of biomass surfaces is shown in Figure 2 for external (a) and internal giant reed surfaces. Table 3 on the other hand showcases the elemental contents in external and internal biomass surfaces. In contrast to the dormant phase (HS-2 and HS-3), higher inorganics were observed during the growing season (HS-4 and HS-1) as seen in Table 3.

The fixed carbon content in Table 2 shows discernible fluctuations across the seasonal variations (HS-1 to HS-4). Notably, in HS-1, the fixed carbon content is 8.81 wt%, showcasing a moderate level. This is succeeded by an increase to 11.2 wt% in HS-2, indicating a higher carbonaceous composition. Conversely, during the HS-3, a slight decrement to 10.9 wt% is observed, although remaining relatively high. Subsequently, in HS-4, there is a noteworthy decline to 8.10 wt%.

3.2 | Structural Components of Giant Reed at Different Seasons

The fibrous composition, described by neutral detergent fiber (NDF) and acid detergent fiber (ADF) content, exhibits notable seasonal variability across the studied seasons (HS-1 to HS-4), as seen in Table 4. During HS-1, NDF content registers at 76.2 ± 1.96 wt%, indicative of a substantial presence of cellulose, hemicellulose, and lignin constituents in biomass. Conversely, ADF content is lower at 52.25 ± 1.41 wt%, suggesting a relatively lesser quantity of holocellulose. Transitioning to HS-2, both NDF and ADF contents exhibit a decline, with

TABLE 1 | Ultimate analysis and higher heating values (HHV) of giant reed.

	Periodic variations			
Parameter	**HS-1**	**HS-2**	**HS-3**	**HS-4**
Ultimate Analysis (wt%)[db]				
Carbon	48.61 ± 0.14	49.69 ± 0.16	49.72 ± 0.14	48.20 ± 0.13
Hydrogen	6.54 ± 0.16	6.37 ± 0.18	6.30 ± 0.18	6.58 ± 0.18
Nitrogen	0.28 ± 0.05	0.29 ± 0.03	0.240 ± 0.03	0.204 ± 0.04
Sulfur	0.025 ± 0.00	0.039 ± 0.01	0.03 ± 0.01	0.015 ± 0.01
Oxygen	44.55 ± 0.20	43.61 ± 0.29	43.71 ± 0.25	45.00 ± 0.23
C/H	7.74 ± 0.17	7.80 ± 0.20	7.89 ± 0.20	7.33 ± 0.18
H/C	0.13 ± 0.00	0.13 ± 0.00	0.13 ± 0.00	0.14 ± 0.00
O/C	0.84 ± 0.44	0.88 ± 0.43	0.88 ± 0.42	0.93 ± 0.51
HHV (MJ/kg)[db]	18.86 ± 0.05	19.73 ± 0.05	19.23 ± 0.04	18.44 ± 0.04

[db]Dry basis.

17571707, 2024, 12, Downloaded from https://onlinelibrary.wiley.com/doi/10.1111/gcbb.70011 by South African Medical Research, Wiley Online Library on [28/11/2024]. See the Terms and Conditions (https://onlinelibrary.wiley.com/terms-and-conditions) on Wiley Online Library for rules of use; OA articles are governed by the applicable Creative Commons License

TABLE 2 | Ultimate analysis of giant reed.

Parameter	Periodic variations			
	HS-1	HS-2	HS-3	HS-4
Proximate analysis (wt%)				
Moisture content[a]	6.14 ± 0.16	5.23 ± 0.13	4.32 ± 0.14	6.21 ± 0.14
Volatile content[db]	86.5 ± 0.73	86.8 ± 0.70	87.2 ± 0.61	85.8 ± 0.58
Ash content[db]	5.69 ± 0.04	2.01 ± 0.02	1.95 ± 0.02	6.10 ± 0.03
Fixed carbon[db]	8.81	11.2	10.9	8.10

[a]Wet basis.
[db]Dry basis.

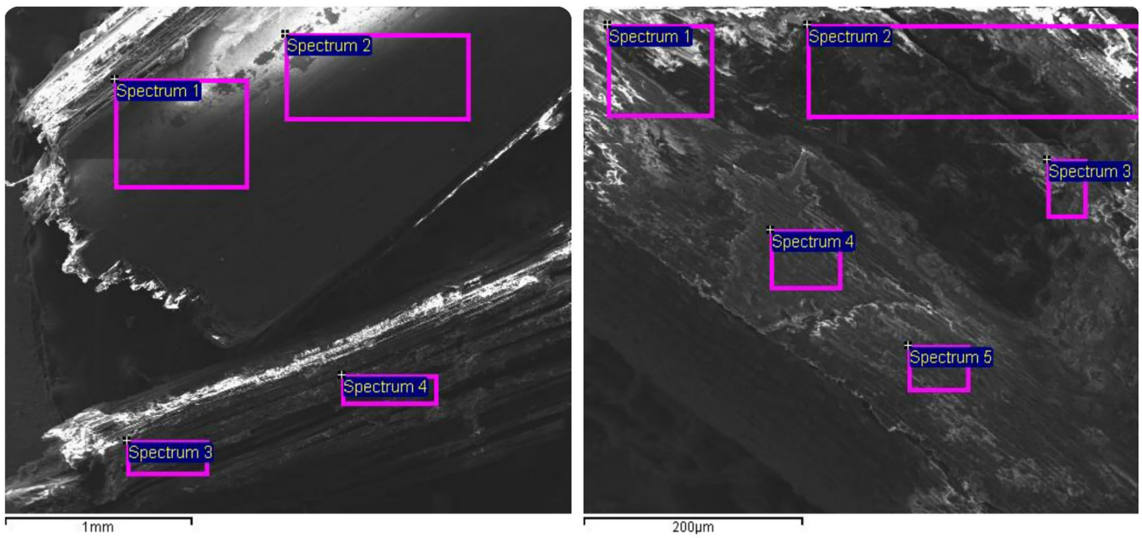


FIGURE 2 | SEM/EDS spectrum of giant reed during HS-2. (a) External surface and (b) internal surface. The elemental analysis primarily identified carbon, oxygen, silicates, and potassium. The EDS analysis was conducted to assess the distribution of these elements across the reed surfaces. Average elemental results are tabulated in Table 3. HS-2: Late autumn season (senescence stage).

TABLE 3 | Internal and external surface elements of giant reed according to SEM/EDS spectrums.

Culm surface	Periodic variations			
	HS-1	HS-2	HS-3	HS-4
External (wt%)[wb]				
Carbon	44.2 ± 3.50	46.5 ± 2.50	47.6 ± 1.70	44.9 ± 3.10
Oxygen	38.5 ± 1.58	38.6 ± 1.77	37.5 ± 1.60	37.9 ± 1.55
Silicates	16.3 ± 0.55	14.14 ± 0.71	14.3 ± 0.69	16.3 ± 0.40
Potassium	1.01 ± 0.01	0.81 ± 0.03	0.73 ± 0.04	0.96 ± 0.01
Internal (wt%)[wb]				
Carbon	55.0 ± 3.15	56.2 ± 4.16	56.9 ± 3.62	54.2 ± 3.02
Oxygen	42.8 ± 2.46	42.7 ± 3.58	42.0 ± 3.37	43.1 ± 2.68
Silicates	2.10 ± 0.45	1.09 ± 0.55	1.06 ± 0.58	2.43 ± 0.47
Potassium	0.10 ± 0.04	0.08 ± 0.05	0.07 ± 0.03	0.29 ± 0.04

[wb]Wet basis.

17571707, 2024, 12, Downloaded from https://onlinelibrary.wiley.com/doi/10.1111/gcbb.70001 by South African Medical Research, Wiley Online Library on [28/11/2024]. See the Terms and Conditions (https://onlinelibrary.wiley.com/terms-and-conditions) on Wiley Online Library for rules of use; OA articles are governed by the applicable Creative Commons License

NDF recording 67.53 ± 1.95 wt% and ADF at 48.54 ± 1.28 wt%. The observed decline was attributed to seasonal variations in plant growth and composition. A comparable trend is observed in the subsequent HS-3 season, where NDF content decreased to 63.75 ± 1.98 wt% and ADF to 47.03 ± 1.21 wt%, indicating a continued reduction in fibrous structural components. Nonetheless, during HS-4, there was a resurgence in fibrous content, with NDF rising to 79.3 ± 1.93 wt% and ADF to 53.97 ± 1.28 wt%.

Several trends were observed in analyzing biomass components across the four seasons (HS-4 to HS-3) (Table 4). Klason lignin content shows variability, with the highest value observed in HS-3 at 19.5 wt% and the lowest in HS-4 at 12.7 wt%. This indicates potential seasonal influences on lignin accumulation. Cellulose content varies across seasons, with the highest value in HS-1 at 38.1 wt% and the lowest in HS-3 at 32.4%, reflecting seasonal changes in plant growth and development. Similarly, hemicellulose content shows fluctuations, with the highest value in HS-1 (23.95 wt%) and the lowest in HS-3 (16.72 wt%).

3.3 | FTIR Of Giant Reed at Different Seasons

The identification of biomass functional groups aids in elucidating the chemical structure of the biomass sample, providing crucial information for its characterization and application during thermochemical conversion. Figure 3 shows the FTIR spectrum of biomass samples.

The functional groups present in biomass can be identified by the different peaks as seen on the spectrum. The broad peak 3333.52 cm^{-1} represents the O-H stretching vibrations of lignin and cellulose present in the biomass sample. In contrast, the peaks at 2918.09 and 2850.21 cm^{-1} are the C-H stretching vibrations, that is, aliphatic compounds in the hemicellulose (Chikouche

TABLE 4 | Structural components and neutral fibers of giant reed.

	Periodic variations			
Parameter	**HS-1**	**HS-2**	**HS-3**	**HS-4**
Fibers (wt%)[db]				
NDF	76.2 ± 1.96	67.53 ± 1.95	63.75 ± 1.98	79.3 ± 1.93
ADF	52.25 ± 1.41	48.54 ± 1.28	47.03 ± 1.21	53.97 ± 1.28
Components (wt%)[db]				
Klason lignin[ef]	15.9 ± 0.93	18.2 ± 0.88	19.5 ± 0.99	12.7 ± 0.89
Lignin	8.46 ± 1.10	12.23 ± 1.08	12.68 ± 1.09	5.11 ± 1.08
Cellulose	38.1 ± 0.27	34.29 ± 0.18	32.4 ± 0.10	40.75 ± 0.17
Hemicellulose	23.95 ± 0.55	18.99 ± 0.67	16.72 ± 0.77	25.33 ± 0.65
Others	23.8	32.47	36.25	20.7

Note: Others = 100-NDF.
[ef]Extractives free.
[db]Dry basis.

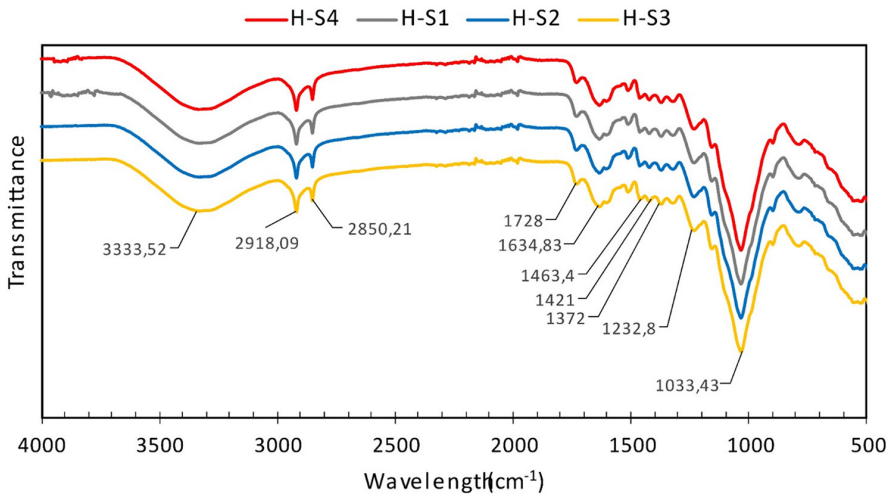


FIGURE 3 | FTIR spectra of giant reed at different periodic variations: Late spring (HS-4), late summer (HS-1), late autumn (HS-2), and late winter (HS-3). Significant peaks include: (1) a broad peak around 333.52 cm^{-1}; (2) peaks around 2919.09 cm^{-1} and 2850.21 cm^{-1}; (3) peaks around 1634.83 cm^{-1} and 1463.4 cm^{-1}.

17571707, 2024, 12, Downloaded from https://onlinelibrary.wiley.com/doi/10.1111/gcbb.70011 by South African Medical Research, Wiley Online Library on [28/11/2024]. See the Terms and Conditions (https://onlinelibrary.wiley.com/terms-and-conditions) on Wiley Online Library for rules of use; OA articles are governed by the applicable Creative Commons License

et al. 2015; Suárez et al. 2023). The peak at 1728 cm^{-1} originates from the C=O stretching vibration of oxygen double bonds due to hemicellulose. The C=O stretching was due to lignin and hemicellulose (Bessa et al. 2020). The aldehyde functionalities are mainly derived from xylose. The 1634.83 and 1463.4 cm-1 peaks may pertain to N-H bending, C=C stretching, and C-H bending vibrations, respectively. The 1421 and 1372 cm-1 peaks are due to O-H bending and S=O stretching resonances, respectively. Thus, the biomass contains carboxylic acid and sulfonate/phenol functionalities. 1232.8 cm^{-1} represents C-O stretching vibrations of lignin and xylan, as well as syringyl ring breathing. The peak at 1033.43 cm^{-1} was attributed to stretching vibrations of S=O/C-N. The peak at 1033.43 cm^{-1} was also due to the presence of cellulose (Martínez-Sanz et al. 2018).

3.4 | Thermal Degradation of Giant Reed at Different Seasons

The information on feasible pyrolysis reaction temperature range and thermal degradation behavior for available biomass materials can be obtained from the thermogravimetric analysis (TGA) and differential thermogravimetry (DTG) profiles. Figure 4a,b represents the TGA and DTG of giant reed during various seasons (HS-4 to HS-3), respectively. The curves show three mass loss partitions/stages. The first stage of degradation represents the loss of moisture or volatilization of light extractives. In Figure 4a, it can be seen that moisture loss occurs between 26°C and 120°C across all seasons with an average loss of 5.48 wt%.

The second stage represents the degradation of cellulose and hemicellulose (holocellulose) at an average temperature range of 225°C to 398°C across all seasons. Pure cellulose, hemicellulose, and lignin have degradation temperatures of 315°C–400°C, 220°C–315°C, and 150°C–900°C, respectively (Yang et al. 2007). The holocellulose degradation during HS-4 and HS-2 occurred at a range of 250°C–398°C and 220°C–360°C, respectively. Meanwhile, in HS-3 and HS-1, the degradation of holocellulose was seen at 260°C–380°C and 260°C–400°C, respectively. That said, it is worth noting that hemicellulose decomposition occurs before cellulose degradation starts at a temperature of 220°C (Bessa et al. 2020). Cellulose degrades at a higher temperature than hemicellulose due to the long polymer of glucose with no branches, thus strengthening its structure and thermal stability. During the second stage (active pyrolysis stage), the average mass loss of around 65 wt% is observed for HS-2 and HS-3, whereas 60 and 59 wt% are observed for HS-1 and HS-4, respectively. Hence, some lipids and proteins also degrade during this stage. The observed mass loss during the second stage corroborates with the estimated values of holocellulose in this current study, although it may include proteins and lipids. The last stage (385°C–800°C) is the continuation of lignin decomposition and carbonization of cross-linked sugar, giving an average weight loss of 10–11 wt% across all seasons. Lignin is composed of aromatic rings with numerous branches bonded by strong chemical bonds; hence, the degradation temperature of lignin covers a wide range (Suárez et al. 2023; Yang et al. 2007). The degradation of other remaining carbonaceous material in biomass is possible during lignin decomposition, going into the final temperature of 800°C. These are the main

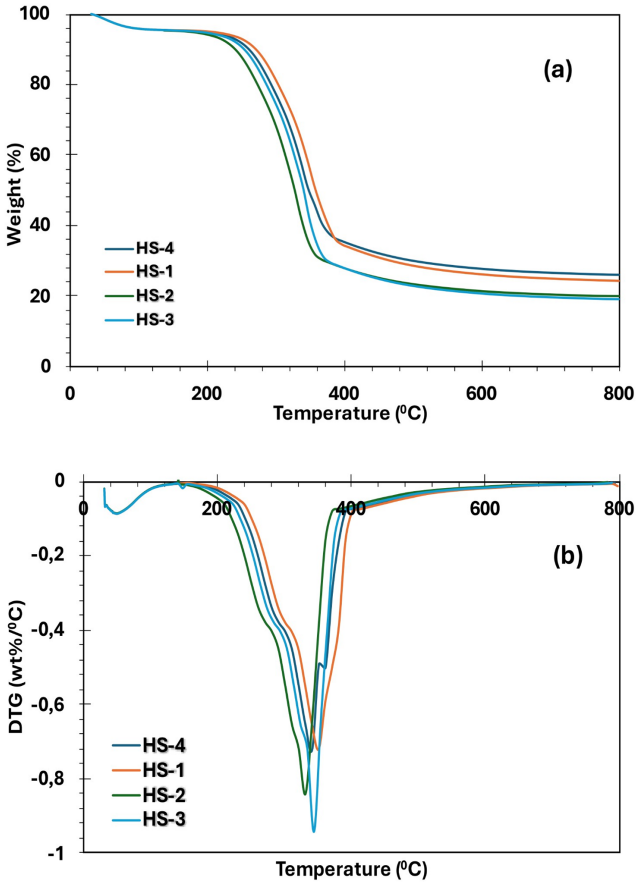


FIGURE 4 | Thermogravimetric analysis of giant reed biomass at different seasons: (a) thermogravimetric analysis (TGA) and (b) differential thermogravimetry (DTG) profiles. TGA: Residual weights after degradation: HS-1: 24%, HS-2: 20%, HS-3: 19%, HS-4: 26%. DTG: Peak mass loss rates at 351°C (HS-1), 331°C (HS-2), 344°C (HS-3), and 341°C (HS-4).

contributors to the char formation (Cheng et al. 2015). The residual weight percentages observed after thermal degradation for the different harvest seasons were HS-1 at 24%, HS-2 at 20%, HS-3 at 19%, and HS-4 at 26%. These results indicate variability in thermal stability among the growth stages, with HS-4 exhibiting the highest residual weight, suggestive of greater char retention and high presence of inorganics, whereas HS-3 showed the lowest residual mass. In Figure 4b, the DTG plot reveals secondary small shoulders observed after the dehydration phase (26°C–120°C), which signify hemicellulose degradation. The temperature range for hemicellulose degradation partially coincides with that of cellulose degradation, resulting in the weight loss rate curve exhibiting a shoulder rather than a distinct peak (Grønli, Várhegyi, and Di Blasi 2002). The profiles in Figure 4b indicate that hemicellulose degradation across all seasonal samples occurs within a temperature range of 220°C–323°C. The prominent peaks within the temperature range of 300°C–400°C signified the degradation of cellulose for all seasons. However, it is worth noting that cellulose degradation started at different temperatures, which was attributed to variations in the structural composition of each biomass sample. Furthermore, high concentrations of low molecular weight compounds (resins and oils) can contribute to faster holocellulose degradation during HS-2 and HS-3 seasons, associated with autumn and winter

17571707, 2024, 12, Downloaded from https://onlinelibrary.wiley.com/doi/10.1111/gcbb.70001 by South African Medical Research, Wiley Online Library on [28/11/2024]. See the Terms and Conditions (https://onlinelibrary.wiley.com/terms-and-conditions) on Wiley Online Library for rules of use; OA articles are governed by the applicable Creative Commons License

harvesting. Hence, the order of degradation for holocellulose was HS-2 < HS-3 < HS-4 < HS-1. Lower hemicellulose contents result in more prominent cellulose peaks. Holocellulose can then decompose simultaneously, forming a more prominent peak (Saffe et al. 2019). The temperatures for maximum mass loss rate are 351°C, 331°C, 344°C, and 341°C for HS-1, HS-2, HS-3, and HS-4, respectively. These maximum mass loss are mainly associated with higher cellulose contents. Furthermore, the observed temperatures of maximum mass loss for giant reed, coincide with the results of Huang et al. (2015). After cellulose degradation, lignin decomposition follows (passive pyrolysis) at a temperature range of 400°C–800°C. During this phase, lignin decomposes without a characteristic peak, possibly due to slight mass loss, which translates to a minimal reaction rate. Thermal degradation rates (−dW/dT), illustrated in Figure 4b, increase from the growing stages (HS-1 and HS-4) to senescence (HS-2), subsequently transitioning into the dormant stage (HS-3). Consequently, the growing stages exhibit a delayed thermal degradation response.

3.5 | Pyrolysis Product Distribution

Pyrolysis products showed variations that reflect seasonal influences, as seen in Figure 5. HS-1 and HS-4 showed the highest bio-oil yields at 42.3 ± 0.95 and 42 ± 0.81 wt%, respectively. Meanwhile, HS-2 and HS-3 yields were averaging at 41 wt%. However, there was a significant difference in the production of aqueous and organic phases, which comprise total liquid yield. HS-1 and HS-4 resulted in higher yields of aqueous phase compared to HS-2 and HS-3.

Conversely, the organic phase demonstrated the opposite trend, with higher yields in HS-2 and HS-3 at 11 ± 0.43 and 11.3 ± 0.42 wt%, respectively (Figure 5). Biochar production was the highest during HS-2 and HS-3, averaging at 24 wt%. Meanwhile, HS-1 and HS-4 yields were slightly lower at 20.5 ± 0.67 and 18 ± 0.76 wt%, respectively. Pyrolysis gas yield ranged from 35 to 49 wt%, with the highest yield obtained during HS-4 (39.7 ± 1.71 wt%) and the lowest yield in HS-2 (34.7 ± 1.81 wt%).

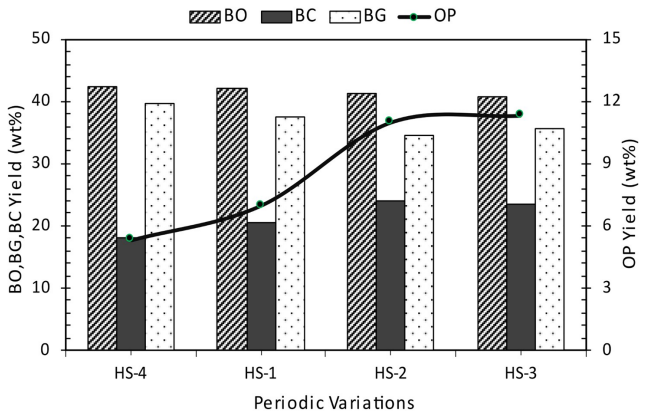


FIGURE 5 | Thermochemical conversion products of giant reed biomass at different harvest seasons: HS-1: Late summer, HS-2: Late autumn, HS-3: Late winter, HS-4: Late spring. Pyrolysis product yields varied by season. BC: biochar yield, BG: pyrolysis gas yield, BO: bio-oil yield, OP: organic phase yield.

3.6 | Properties of Bio-Oil Organic Phase

The analyses of bio-oil samples collected during different seasonal variations (HS-1, HS-2, HS-3, and HS-4) are tabulated in Table 5. These analyses exhibited discrepancies in both proximate and ultimate composition. Moisture content showed a slight variation, with HS-4 displaying the highest value at 9.95 ± 0.05 wt% as expected since biomass was harvested during semi-early stages of growth.

Pertaining to the ultimate analysis, significant differences were noted in the carbon, hydrogen, nitrogen, sulfur, and oxygen content across all seasons. HS-2 exhibited the highest carbon content at 71.18 ± 0.75 wt%, whereas HS-4 had the highest oxygen content at 28.62 ± 0.67 wt%. Hydrogen content varied from 7.34 ± 0.07 wt% in HS-4 to 7.99 ± 0.08 wt% in HS-3. Nitrogen content ranged from 0.12 ± 0.02 wt% in HS-4 to 0.55 ± 0.02 wt% in HS-2, with considerable disparity. The properties of the bio-oil samples, that is, kinematic viscosity, density, total acid number (TAN), dynamic viscosity, and higher heating value (HHV), also varied with seasons. HS-1 and HS-4 demonstrated higher TAN values at 58.1 ± 1.26 and 59.2 ± 1.31 mgKOH/g, respectively, compared to HS-2 (54.3 ± 1.25) and HS-3 (53.2 ± 1.23), indicating differences in acidity levels. The reed harvested during the dormant phase showed lower acidity than the one harvested during the active growth phase. HS-2 and HS-3 showed low kinematic viscosity at 53.2 ± 1.15 and 54.4 ± 1.24 mm2/s, respectively. Conversely, higher viscosity was observed during HS-4 and HS-1. Meanwhile, the density is consistent for HS-4 and HS-1, followed by another consistency between HS-2 and HS-3. Additionally, HHV values were higher for HS-2 and HS-3 when compared to HS-1 and HS-4, suggesting variations in the energy content of the bio-oil samples. It ranged from 19.4 ± 0.03 MJ/kg in HS-4 to 22.6 ± 0.04 MJ/kg in HS-2.

The Van Krevelen plot (Figure 6) is a powerful tool for assessing the molecular composition of various fuels, specifically through the analysis of hydrogen-to-carbon (H/C) and oxygen-to-carbon (O/C) molar ratios. This study evaluated and compared the ratios for biomass and bio-oil organic phase (BOP) to crude oil and gasoline across different harvest seasons (HS-4 to HS-3). The BOP exhibits a range of O/C ratios from 0.22 to 0.34 and H/C ratios from 1.32 to 1.45. Crude oil presents an O/C ratio of 0.0017 and an H/C ratio of 1.3, reflecting its highly carbon-rich and low-oxygen nature (Panwar and Paul 2021). Similarly, gasoline has an O/C ratio of 0 and an H/C ratio of 1.79, emphasizing its complete removal of oxygen, which is characteristic of refined petroleum products (Hu and Gholizadeh 2020). The lowest O/C ratio for BOP was obtained during the senescence-dormant phase (HS-2 and HS-3).

3.7 | GCMS Analysis of Bio-Oil Organic Phase

The GCMS analysis of bio-oil samples obtained during seasonal variations revealed significant distinctions in the composition and distribution of organic compounds (Figure 7). The identified compounds were grouped as aldehydes, ketones, furans, phenolics, olefins, sugars, and others. Furthermore, "others" were a classification of other compound groups in bio-oil, namely, amines, aromatics, esters, acids, alcohols, aliphatic,

17571707, 2024, 12, Downloaded from https://onlinelibrary.wiley.com/doi/10.1111/gcbb.70001 by South African Medical Research, Wiley Online Library on [28/11/2024]. See the Terms and Conditions (https://onlinelibrary.wiley.com/terms-and-conditions) on Wiley Online Library for rules of use; OA articles are governed by the applicable Creative Commons License

TABLE 5 | Proximate, ultimate analysis, and properties of BOP.

Parameter	Gasoline	Periodic variations			
		HS-1	HS-2	HS-3	HS-4
Proximate analysis (wt%)					
Moisture content[a]	***	9.80 ± 0.15	9.82 ± 0.14	9.79 ± 0.19	9.95 ± 0.05
Ultimate analysis (wt%)[db]					
Carbon	86.00	65.00 ± 0.75	71.18 ± 0.75	69.65 ± 0.70	63.78 ± 0.73
Hydrogen	12.80	7.84 ± 0.08	7.83 ± 0.08	7.99 ± 0.08	7.34 ± 0.07
Nitrogen	0.000	0.24 ± 0.04	0.55 ± 0.02	0.52 ± 0.03	0.12 ± 0.02
Sulfur	1.000	0.06 ± 0.02	0.01 ± 0.02	0.04 ± 0.02	0.14 ± 0.03
Oxygen	< 0.20	26.86 ± 0.67	20.44 ± 0.66	21.8 ± 0.53	28.62 ± 0.67
H/C	1.790	1.45 ± 0.00	1.32 ± 0.00	1.38 ± 0.00	1.38 ± 0.00
O/C	0.002	0.31 ± 0.00	0.22 ± 0.01	0.23 ± 0.00	0.34 ± 0.00
Properties[ar]					
K. Viscosity (cSt) 40°C	0.5 at 20°C	66.6 ± 1.05	53.2 ± 1.15	54.4 ± 1.24	67.8 ± 1.35
Density (g/cm^3) 40°C	0.76 at 15°C	1.18 ± 0.00	1.14 ± 0.00	1.14 ± 0.00	1.18 ± 0.00
TAN (mgKOH/g)	0.05–0.2	58.1 ± 1.26	54.3 ± 1.25	53.2 ± 1.23	59.2 ± 1.31
D. Viscosity (mPa.s) 40°C	0.38 at 15°C	78.4 ± 1.05	60.6 ± 1.15	62.0 ± 1.24	80.0 ± 1.35
HHV (MJ/kg)[db]	45.70	20.8 ± 0.03	22.6 ± 0.04	22.0 ± 0.02	19.4 ± 0.03

[a]Wet basis.
[ar]As received.
[db]Dry basis.

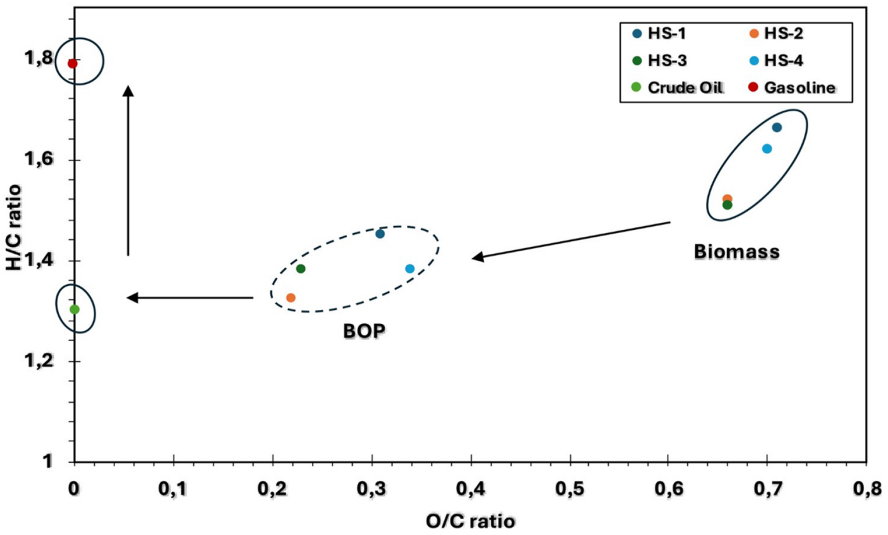


FIGURE 6 | Van Krevelen plot of giant reed biomass and bio-oil organic phase (BOP) compared to crude oil and gasoline. The plot illustrates the hydrogen-to-carbon (H/C) and oxygen-to-carbon (O/C) molar ratios, providing insights into the molecular composition of giant reed biomass and its bio-oil organic phase (BOP) in comparison to crude oil and gasoline. [late spring (HS-4), late summer (HS-1), late autumn (HS-2), and late winter (HS-3)].

ethers, organosilicon, nitriles, nucleoside, alkoxysilanes, and cyclopentanetriols.

Pyrolysis incorporates complex reactions owing to the degradation of hemicellulose, cellulose, and lignin. Decomposition of cellulose and hemicellulose forms 1-hydroxy-2-propanone, acetic acid, anhydro sugars, furans, and levoglucosan, among other compounds. Meanwhile, phenolics, aldehydes, ketones, guaiacols, alcohols, and carboxylic acids come from lignin decomposition (Guilhaume, Schuurman, and Geantet 2021).

17571707, 2024, 12, Downloaded from https://onlinelibrary.wiley.com/doi/10.1111/gcbb.70001 by South African Medical Research, Wiley Online Library on [28/11/2024]. See the Terms and Conditions (https://onlinelibrary.wiley.com/terms-and-conditions) on Wiley Online Library for rules of use; OA articles are governed by the applicable Creative Commons License

Aldehydes were significantly higher during HS-1 at 5.46% compared to 0.31% during HS-4. Phenolics demonstrated significant variability across seasons, with HS-4 exhibiting the highest content at 70.49% and HS-1 showing the lowest at 31.1%. In HS-2 and HS-3, the phenolic compounds were relatively high at 65.21% and 55%, respectively. Ketones showed relatively consistent levels across all seasons, with HS-3 exhibiting the highest percentage at 18.79%, followed by HS-4 at 15.29%. Furan derivatives were elevated in HS-1 (12.31%) followed by HS-3 at 3%, suggesting variations in biomass characteristics over various seasons. However, during HS-2 and HS-4, furans remained relatively flat at 0.49 and 1.28%, respectively. Olefins were predominantly present in HS-4, constituting 5.32% of the composition.

The sugars were highest in HS-1 at 21.87%, with a decrease in HS-2 and HS-3 (6.36% and 3.71%, respectively). During HS-4, no sugar compound was detected. 1,4:3,6-Dianhydro-α-d-glucopyranose, the dehydrated form of levoglucosan, was also obtained in bio-oils during HS-1, HS-2, and HS-3.

3.8 | GCMS Analysis on the Distribution of "Others"

The "others" compounds are shown in Figure 8, which further showcases the compound groups for different seasons. The alcohols were found in HS-2 and HS-3 at 0.87% and 2.22%, respectively. Similarly, the ether groups were 0.72 and 1.83% for HS-2 and HS-3, respectively. The amine and ester groups were present in all seasons. However, HS-1 was rich in esters, and HS-4 was rich in amines. The increase in esters and amines was HS-1 > HS-3 > HS-4 > HS-2 and HS-1 > HS-4 > HS-3 > HS-2, respectively. The acids dominated during HS-2 at 4.96%, followed by 0.58% in HS-4. Aliphatic compounds were present in HS-1 and HS-3 at 1.24 and 3.06%, respectively.

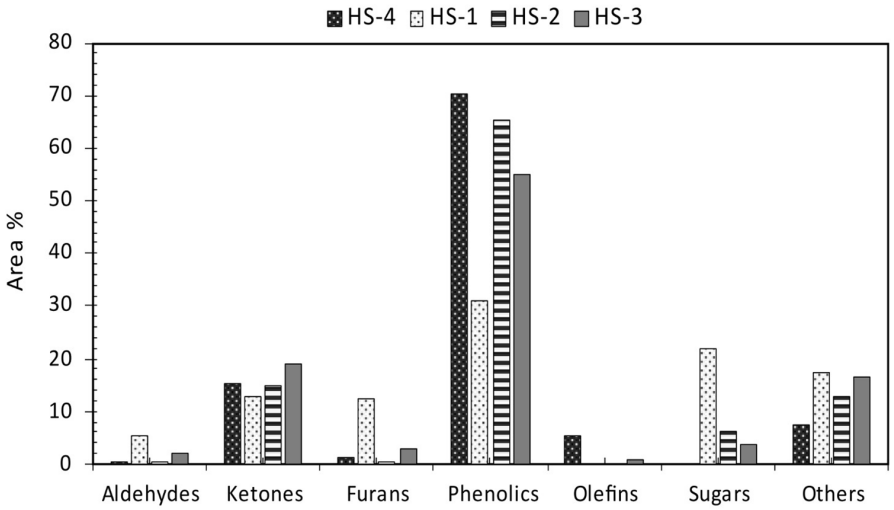


FIGURE 7 | Functional groups of bio-oil organic phase (BOP) as detected by GC–MS at different seasonal variations. The identified compounds were categorized into aldehydes, ketones, furans, phenolics, olefins, sugars, and others, which were identified based on their retention times, mass spectra, and Area%. [late spring (HS-4), late summer (HS-1), late autumn (HS-2), and late winter (HS-3)].

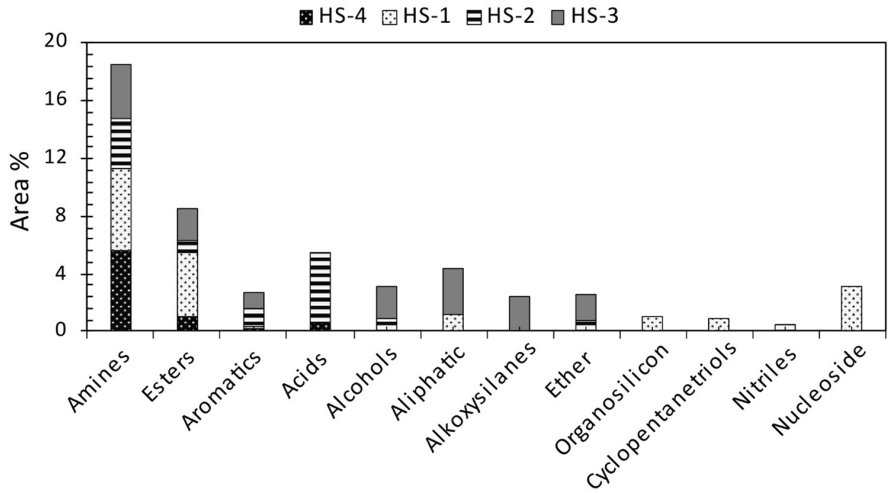


FIGURE 8 | Distribution of "Others" functional groups detected by GC–MS in bio-oil organic phase (BOP) at different harvest seasons. The "Others" category includes amines, esters, acids, alcohols, aliphatic compounds, and more. [late spring (HS-4), late summer (HS-1), late autumn (HS-2), and late winter (HS-3)].

17571707, 2024, 12, Downloaded from https://onlinelibrary.wiley.com/doi/10.1111/gcbb.70011 by South African Medical Research, Wiley Online Library on [28/11/2024]. See the Terms and Conditions (https://onlinelibrary.wiley.com/terms-and-conditions) on Wiley Online Library for rules of use; OA articles are governed by the applicable Creative Commons License

3.9 | Energy Density of Bio-Oil Organic Phase

The biomass energy distribution (Figure 9) of the bio-oil organic phase was determined from the ratio of the heating values. The energy density gives the biomass energy share that is respective to the bio-oil organic phase. As previously discussed, the highest organic phase yield was obtained during HS-3 and HS-2, whereas the lowest yield was observed in HS-4. The high organic phase yields correlated with high lignin content during HS-3 and HS-2. On energy distribution, approximately 14% of initial HHV was converted into the organic phase during HS-3 and HS-2. Meanwhile, 5.72% and 11% of the initial HHV were converted into the organic phase during HS-4 and HS-1, respectively.

3.10 | Characterization of Non-condensable Gases

The pyrolysis gas/non-condensable gases were collected and analyzed during biomass degradation at different seasonal variations (HS-4 to HS-3). The results of the analyzed pyrolysis gas samples are shown in Figure 10. The analysis of the pyrolysis gas mixture identified the following gases: hydrogen (H_2), nitrogen (N_2), carbon monoxide (CO), carbon dioxide (CO_2), oxygen (O_2), ethene (C_2H_4), ethane (C_2H_6), others (C_xH_y), and methane (CH_4). Nitrogen, carbon monoxide, carbon dioxide, and methane were the predominant gases based on the identified gases. Nitrogen had the highest concentration by volume compared to other gases, which was attributed to nitrogen being used as the carrier gas during pyrolysis. Carbon dioxide and carbon monoxide had the highest concentration by volume during HS-4. Meanwhile, during HS-1, the highest concentration of hydrogen was observed and the lowest carbon dioxide concentration compared to other seasons.

4 | Discussion

4.1 | Biomass Fuel Properties

The observed elemental shifts highlighted the significance of biomass pyrolysis aligned with seasonal variations for optimal bio-oil quality and yield. The heating value of cane biomass is

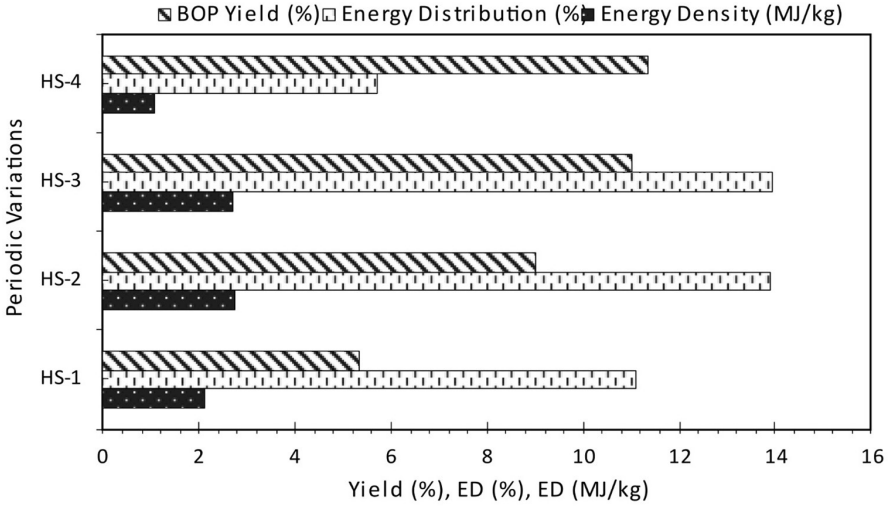


FIGURE 9 | Yield (%), energy density [ED (MJ/kg)], and energy distribution [ED (%)] of bio-oil organic phase (BOP) at different seasonal variations: Late spring (HS-4), late summer (HS-1), late autumn (HS-2), and late winter (HS-3).

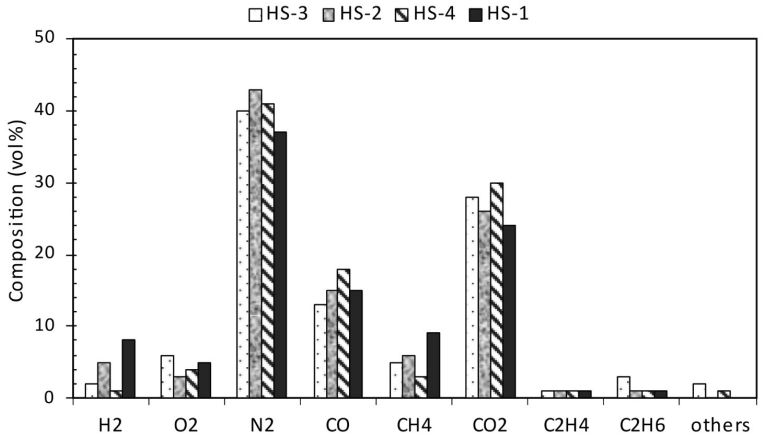


FIGURE 10 | Pyrolysis gas distribution during thermochemical conversion of giant reed harvested at different seasons: Late spring (HS-4), late summer (HS-1), late autumn (HS-2), and late winter (HS-3). The gas composition, represented as Vol%, included hydrogen (H_2), nitrogen (N_2), carbon monoxide (CO), carbon dioxide (CO_2), oxygen (O_2), ethene (C_2H_4), ethane (C_2H_6), methane (CH_4), and other CxHy compounds.

17571707, 2024, 12, Downloaded from https://onlinelibrary.wiley.com/doi/10.1111/gcbb.70011 by South African Medical Research, Wiley Online Library on [28/11/2024]. See the Terms and Conditions (https://onlinelibrary.wiley.com/terms-and-conditions) on Wiley Online Library for rules of use; OA articles are governed by the applicable Creative Commons License

higher than grass biomass and comparable to woody biomass (Nordin 1994). This supported the utilization of giant reed biomass for bioenergy applications. Reduced oxygen contents directly indicated that HS-2 and HS-3 seasons are sufficient for giant reed to reach a high level of HHV. Moreover, the low sulfur and nitrogen contents indicated the possibility of improved quality of bio-oil, that is, it may result in low emissions of sulfur and nitrogen oxides when burnt.

The higher volatile content in HS-3 indicated that biomass can release more volatile compounds during pyrolysis, which results in higher bio-oil yields. Meanwhile, the lower moisture content seen during HS-3 indicated that biomass harvested in this season may require less energy for drying before pyrolysis. The observed trend in moisture content variations coincides with the results of Liu et al. (2016). Lower moisture content in biomass is essential for reducing transportation and storage costs; thus, HS-2 and HS-3 are optimal harvest seasons for low moisture content.

These variations in ash content showed changes in the mineral composition (inorganics) of the biomass, likely influenced by factors such as soil conditions and weather patterns. Additionally, the variations in ash content can be attributed to the translocation of nutrients from the above-ground plant to the roots at the end of the growing season (Smith and Slater 2011). The observed trend of the ash content correlated with the presence of silicates and potassium, as seen in Table 3. The inorganics (silicates and potassium) were higher at the external surface than at the internal surface. Silicates and potassium were highest during HS-4 and HS-1 on internal and external surfaces, coinciding with the ash content.

Giant reed starts to senescence in autumn/winter or lose their foliage, which results in biomass loss (Liu et al. 2016). Similarly, switchgrass, miscanthus, and reed canary plants experience biomass loss of around 20% in the autumn/winter season (Monti, Di Virgilio, and Venturi 2008). Giant reed foliage contains more inorganics, which results in higher ash content (Ge et al. 2016). Hence, the current study only focused on the culm/stem of the giant reed. In contrast to HS-4 and HS-1, fouling problems during pyrolysis due to high inorganics are minimal for HS-3 and HS-2. Higher ash content is undesirable as it directly influences the yield and quality of bio-oil. Reduction in ash content correlated with increased organic content, thus improving bio-oil quality post-pyrolysis.

Fixed carbon content is a pivotal determinant of biochar yield and quality, with higher levels typically correlating with enhanced carbon sequestration potential and thermochemical conversion efficiency. HS-3 and HS-2 are associated with periods of dormancy, hence the observed trends in the biomass proximate analyses. On the other hand, HS-4 and HS-1 are associated with the growing season. The results showed that HS-3 and HS-2 are desirable harvest seasons for giant reed for thermochemical conversion applications when BOP is the desired product. The observed variations in biomass proximate and ultimate analyses were attributed to intrinsic changes in biomass composition, environmental conditions, and growth patterns across seasons.

4.2 | Structural Components of Biomass

The observed variations in NDF and ADF content emphasize the influence of seasonal factors on biomass structural composition, which is crucial for optimizing the pyrolysis process. The fibrous materials, particularly cellulose, hemicellulose, and lignin, play a pivotal role in determining the product distribution and properties during thermochemical conversion. The decline in fibrous components (NDF and ADF) from HS-1 to HS-3 can be attributed to seasonal growth patterns, where biomass composition becomes less fibrous as the plant matures and lignification progresses.

The resurgence in fibrous content during HS-4, with an increase in NDF and ADF, indicates a return to higher cellulose and hemicellulose levels, which may be tied to the growing season and active plant processes. The fluctuation in cellulose and hemicellulose content, as observed between HS-1 and HS-3, aligned with the general understanding that cellulose and hemicellulose decline as giant reed matures. The significant decrease in hemicellulose from HS-4 to HS-3 was likely due to the lignification effect, which involves the conversion of hemicellulose into more rigid lignin structures.

Klason lignin content also demonstrated seasonal variability, with the highest values observed in HS-3, suggesting that lignin accumulation peaks during this period. These fluctuations reflect seasonal influences on biomass composition, which impacts its suitability for BOP production via pyrolysis. The observed trends are consistent with literature values: Neto et al. (1997) reported that the culm of giant reed had 3 wt% ash, 17.2 wt% lignin, and 58.8 wt% holocellulose, which closely aligns with the composition seen in HS-2. Suárez et al. (2023) found similar cellulose, hemicellulose, and lignin estimates for giant reed, further supporting the seasonal trends observed in this study. Additionally, Liu et al. (2016) provided polymer estimations over 4 months, with cellulose ranging between 29 and 31 wt%, hemicellulose between 14 and 16 wt%, and lignin between 16 and 18 wt%, further emphasizing the variability in biomass composition across seasons.

4.3 | Pyrolysis Product Distribution

The disparity in the aqueous and organic phase (OP) yields could arise from varied biomass compositions affecting phase separation efficiencies during pyrolysis. HS-1 and HS-4 may yield higher aqueous fractions due to elevated moisture content, whereas HS-2 and HS-3 exhibited greater organic phase yields, possibly due to differences in extractable organic compounds. Furthermore, the observed increase in the aqueous phase during HS-4 and HS-1 could also be attributed to higher oxygen content. High oxygen content promotes dehydration reactions during pyrolysis, which forms water as a product (Rangel et al. 2023). The elevated biochar yields in HS-2 and HS-3 were attributed to potential factors such as higher lignin content and denser biomass structure (increased fixed carbon content), which favors biochar formation during pyrolysis. Higher volatile content in HS-1 and HS-2 correlated with increased pyrolysis gas yields due to greater gasification potential during pyrolysis.

17571707, 2024, 12, Downloaded from https://onlinelibrary.wiley.com/doi/10.1111/gcbb.70001 by South African Medical Research, Wiley Online Library on [28/11/2024]. See the Terms and Conditions (https://onlinelibrary.wiley.com/terms-and-conditions) on Wiley Online Library for rules of use; OA articles are governed by the applicable Creative Commons License

This results in higher gas production, contrasting with lower volatile content in HS-3 and HS-4, which leads to reduced pyrolysis gas yields. In the current study, biochar was lower than pyrolysis gas for all seasons, this observation was in contrast with the work reported by Temiz et al. (2013). The authors reported liquid, solid, and gas yields of 45, 30, and 25 wt% during the thermal degradation of giant reed. These disparities were attributed to different operating conditions during pyrolysis.

4.4 | BOP Versus Gasoline and Crude Oil

Although this study did not focus on upgrading BOP to fuel-range hydrocarbons, comparing the O/C and H/C ratios to crude oil and gasoline was necessary to understand the best BOP based on seasonal variations. The O/C ratios indicated that BOP retains a significant oxygen content compared to conventional fossil fuels, which typically have much lower O/C ratios.

Furthermore, the O/C and H/C ratios also highlighted the loss of functional groups that contain oxygen and hydrogen, such as –OH, –COOH, and $–CH_3$, likely due to dehydration and deoxygenation reactions during pyrolysis. The low O/C ratio correlated with the reduction of oxygen-containing functional groups through the decrease in oxygen content from the active growth stage (HS-4 and HS-1) to the senescence-dormant phase (HS-2 and HS-3). The higher O/C ratios in BOP compared to both crude oil and gasoline indicate a less mature fuel composition, suggesting that BOP may still contain a significant proportion of polar functional groups, which can influence its reactivity and suitability as a biofuel. This is consistent with previous findings highlighting that bio-oil hydroxyl and carboxyl functional groups contribute to higher oxygen content (Bridgwater 2012).

The H/C ratios of BOP in the current study ranged from 1.32 to 1.45; these are lower than those of gasoline (1.79) but comparable to crude oil (1.3). Higher H/C ratios are desired for the fuel to be more efficient through reducing CO emissions, whereas lower H/C ratios are undesirable since it translates to more aromatics, thus making bio-oil less reactive. This also induces more coking during bio-oil upgrading via hydrodeoxygenation. The lower H/C ratio in BOP indicated a higher degree of unsaturation and potential functionalization than gasoline, primarily composed of saturated hydrocarbons. The reduced H/C ratios for BOP were attributed to hydrogen being transformed into water and recovered in the aqueous phase of bio-oil. Other compounds that carry hydrogen away from the organic phase into the aqueous phase include alcohols, carboxylic acids, aldehydes, and ketones.

Additionally, some hydrogen was also lost through non-condensable gases and biochar. This characteristic suggests that while BOP may be suitable for energy applications, further upgrading or refining may be necessary to improve its fuel properties, particularly regarding stability and energy density. Since only BOP was considered in the current study, it supported the prospect of decreasing H/C ratios. The Van Krevelen plot analysis revealed that the BOP retains a higher O/C ratio and lower H/C ratio than gasoline and crude oil, indicating its potential for further refinement to enhance fuel quality.

4.5 | Compounds of BOP

Aldehydes were significantly higher during HS-1, indicating potential differences in biomass degradation kinetics that favored the formation of aldehyde compounds during this phase. Phenolics demonstrated significant variability across seasons, with HS-4 exhibiting the highest content. This was reflective of seasonal fluctuations in lignin and cellulose compositions. Bio-oil from HS-4 was mainly in the aqueous phase, with the high area% of phenolics mainly due to polar phenolic compounds. Phenolic content decreased with plant maturity despite phenolics being primarily derived from lignin, which is thought to stop lignification during dormant phases. This suggested that the constituent structure of the biomass highly influences the distribution of pyrolysis products (Azeez et al. 2010). The application of phenols includes manufacturing renewable resin, which can replace conventional petroleum-based phenol.

Ketones showed consistent levels across all seasons, with HS-3 exhibiting the highest percentage, suggesting that these compounds form esters when oxidized. Phenolics and ketones are oxygenated compounds that significantly lower the heating value of bio-oil (Arazo et al. 2017). Furan derivatives were elevated in HS-1 and HS-3, suggesting variations in biomass characteristics. However, during HS-2 and HS-4, furans remained relatively flat. This indicates that furans, which are typical products of cellulose and lignin decomposition, are influenced by the specific thermal degradation pathways of the biomass (Cheng et al. 2015).

Olefins were predominantly present in HS-4, indicative of differences in the thermal degradation pathways of biomass constituents that favored the formation of these compounds during this phase. The high sugar content in HS-1 was due to the degradation of biomass carbohydrates during pyrolysis. In contrast, the decrease in sugars during HS-2, HS-3, and HS-4 was attributed to fission and disproportionation, leading to the formation of furans and acids. The main sugar compound that was obtained in bio-oils was levoglucosan from the decomposition of cellulose. It is formed during a depolymerization reaction due to transglycosylation at 300°C (Azeez et al. 2010). Additionally, the high content of inorganics promoted glucose fragmentation rather than polymerization, contributing to the reduction of sugar compounds. The observed seasonal variations in bio-oil compounds underline the importance of determining the desired product before harvesting biomass for thermochemical conversion.

Acid compounds and their derivatives were formed due to the decomposition of hemicellulose. The nitrogenous compounds were attributed to the heterocyclic ring-containing compounds in the biomass (Kumar, Upadhyay, and Mishra 2022). Amines were attributed to the significance of nitrogen atoms during plant growth. Amines are not desirable as fuel; however, amine solvents are essential in scrubbing carbon dioxide from flue gas via amine-based post-combustion capture (PCC), thus preventing air pollution. The presence of various compounds highlighted the complex nature of bio-oil composition and the relationship of factors influencing pyrolysis products during different seasons.

17571707, 2024, 12, Downloaded from https://onlinelibrary.wiley.com/doi/10.1111/gcbb.70001 by South African Medical Research, Wiley Online Library on [28/11/2024]. See the Terms and Conditions (https://onlinelibrary.wiley.com/terms-and-conditions) on Wiley Online Library for rules of use; OA articles are governed by the applicable Creative Commons License

4.6 | Energy Distribution of BOP and Non-condensable Gas Composition

The HHV values of BOP correlated with the variations in BOP oxygen and water contents. The results emphasized the significant impact of seasonal variations on the composition and properties of bio-oil. Hence, it was evident that HS-2 and HS-3 showed improved BOP energy content compared to HS-1 and HS-4. From an energy yield perspective, it is crucial to recognize that the calculation of percentage energy density may be erroneous if the yield of the pyrolysis liquid is solely attributed to the organic phase without correctly differentiating between the organic and aqueous phases. This increases energy density percentages, accounting for the aqueous phase yield. Furthermore, the pyrolysis liquid phases have distinct heating values; thus, it is necessary to account for organic phase yield when determining the energy density. The aqueous phase needs to be accounted for separately due to distinct heating values compared to the organic phase.

The release of carbon dioxide during the thermal degradation of biomass was mainly attributed to the holocellulose and lignin (Yang et al. 2007). In addition, the degradation of monosaccharide and polysaccharide fractions of hemicellulose are the dominant contributors to the formation of carbon monoxide and carbon dioxide (Gaur and Reed 2020). Biochar oxidation is another contributor to increased carbon dioxide and carbon monoxide (Baker et al. 2005; Lee and Fasina 2008). This explains the highest carbon dioxide and carbon monoxide concentrations during HS-4 (growing phase).

5 | Conclusions

Harvest time significantly impacts the fuel properties of lignocellulosic biomass, specifically giant reed. Elemental analysis revealed that carbon and hydrogen contents remained relatively stable, while inorganic materials peaked during the active growth stage (HS-1 and HS-4), contributing to higher ash content. Thermogravimetric behavior also supported the prospect of higher inorganics during active growth stages. The HHV values of biomass increased from 18.44 ± 0.04 to 19.73 ± 0.05 MJ/kg from the active growth to the senescence-dormant phase (HS-2 and HS-3). While holocellulose content decreased, lignin content increased, with fixed carbon being the highest during the senescence-dormant phase. Higher ash content correlated with lower bio-oil organic phase and pyrolysis gas yields, whereas lower ash content yielded higher yields. The organic phase yield increased from the active growth stage to the senescence-dormant phase, significantly linked to lignification ($R^2 = 0.97$). Properties of the bio-oil organic phase improved during the senescence-dormant period, with viscosity and total acid number decreasing alongside increasing HHV values. The O/C ratio varied, reaching its lowest during the senescence-dormant phase. The HHV values of the BOP ranged from 19.4 ± 0.03 to 22.6 ± 0.02 MJ/kg during active growth to senescence-dormant periods. Therefore, harvesting giant reed in autumn optimizes biomass and BOP properties, minimizes carbon emissions from incineration, and mitigates flooding issues from dormant plant blockages.

Author Contributions

Manqoba Shezi: conceptualization, data curation, formal analysis, investigation, methodology, writing – original draft. **Sammy Lewis Kiambi:** funding acquisition, resources, supervision, validation, writing – review and editing. **Yusuf Makarfi Isa:** formal analysis, resources, supervision, validation, writing – review and editing.

Acknowledgments

The authors wish to acknowledge the financial support from the Durban University of Technology (DUT) and the National Research Foundation (NRF) toward this research. The gratitude is also extended to the School of Chemical and Metallurgical Engineering at the University of Witwatersrand (WITS), the Department of Chemistry at the University of Cape Town (UCT), and CALEB laboratories for providing sophisticated analyses for the current study. Last but not least, the authors wish to thank Mr. Vishnu Kribagaran Moodley for endless support on the lab supplies and the design of the pyrolysis unit.

Conflicts of Interest

The authors declare no conflicts of interest.

Data Availability Statement

The data that support the findings of this study are openly available in Zenodo at https://doi.org/10.5281/zenodo.14055297.

References

Ahmed, G., and N. Kishore. 2023a. "Fuel Phase Extraction From Pyrolytic Liquid of *Azadirachta indica* Biomass Followed by Subsequent Characterization of Pyrolysis Products." *Renewable Energy* 219: 119460.

Ahmed, G., and N. Kishore. 2023b. "Separation and Extensive Evaluation of Properties of Fuel and Non-Fuel Portions of Pyrolytic Bio-Oil Obtained From *Erythrina indica* Biomass." *Journal of Renewable and Sustainable Energy* 15, no. 3: 1–9.

Ahmed, G., and N. Kishore. 2024. "Synergistic Effects on Properties of Biofuel and Biochar Produced Through Co-Feed Pyrolysis of Erythrina Indica and *Azadirachta indica* Biomass." *Renewable Energy* 227: 120508.

Aravind, S. V., G. Ahmed, and N. Kishore. 2023. "Pyrolysis of *Delonix regia* Using Metal Oxide Catalysts and Solvent Effect on Fuel Fraction of Bio-Oil." *Results in Engineering* 17: 100876.

Arazo, R. O., D. A. D. Genuino, M. D. G. de Luna, and S. C. Capareda. 2017. "Bio-Oil Production From Dry Sewage Sludge by Fast Pyrolysis in an Electrically-Heated Fluidized Bed Reactor." *Sustainable Environment Research* 27, no. 1: 7–14.

Auersvald, M., B. Shumeiko, M. Staš, D. Kubička, J. Chudoba, and P. Šimáček. 2019. "Quantitative Study of Straw Bio-Oil Hydrodeoxygenation Over a Sulfided NiMo Catalyst." *ACS Sustainable Chemistry & Engineering* 7, no. 7: 7080–7093.

Awasthi, M. K., T. Sar, S. C. Gowd, et al. 2023. "A Comprehensive Review on Thermochemical, and Biochemical Conversion Methods of Lignocellulosic Biomass Into Valuable End Product." *Fuel* 342: 127790.

Azeez, A. M., D. Meier, J. r. Odermatt, and T. Willner. 2010. "Fast Pyrolysis of African and European Lignocellulosic Biomasses Using Py-GC/MS and Fluidized Bed Reactor." *Energy & Fuels* 24, no. 3: 2078–2085.

Ba, Y., F. Liu, X. Wang, and J. Yang. 2020. "Pyrolysis of C3 Energy Plant (*arundo donax*): Thermogravimetry, Mechanism, and Potential Evaluation." *Industrial Crops and Products* 149: 112337.

Baker, R. R., S. Coburn, C. Liu, and J. Tetteh. 2005. "Pyrolysis of Saccharide Tobacco Ingredients: A TGA–FTIR Investigation." *Journal of Analytical and Applied Pyrolysis* 74, no. 1–2: 171–180.

17571707, 2024, 12, Downloaded from https://onlinelibrary.wiley.com/doi/10.1111/gcbb.70001 by South African Medical Research, Wiley Online Library on [28/11/2024]. See the Terms and Conditions (https://onlinelibrary.wiley.com/terms-and-conditions) on Wiley Online Library for rules of use; OA articles are governed by the applicable Creative Commons License

Bessa, W., D. Trache, M. Derradji, et al. 2020. "Characterization of Raw and Treated *Arundo donax* L. Cellulosic Fibers and Their Effect on the Curing Kinetics of Bisphenol A-Based Benzoxazine." *International Journal of Biological Macromolecules* 164: 2931–2943.

Bridgwater, A. V. 2012. "Review of Fast Pyrolysis of Biomass and Product Upgrading." *Biomass and Bioenergy* 38: 68–94.

Çağlar, A., and A. Demirbaş. 2002. "Conversion of Cotton Cocoon Shell to Hydrogen Rich Gaseous Products by Pyrolysis." *Energy Conversion and Management* 43, no. 4: 489–497.

Cheng, L., S. Adhikari, Z. Wang, and Y. Ding. 2015. "Dynamic Variation of Fuel Properties of Tonkin Cane (*Pseudosasa amabilis*) During Maturation." *Energy & Fuels* 29, no. 4: 2408–2415.

Chikouche, M. D. L., A. Merrouche, A. Azizi, M. Rokbi, and S. Walter. 2015. "Influence of Alkali Treatment on the Mechanical Properties of New Cane Fibre/Polyester Composites." *Journal of Reinforced Plastics and Composites* 34, no. 16: 1329–1339.

Corno, L., R. Pilu, and F. Adani. 2014. "*Arundo donax* L.: A Non-food Crop for Bioenergy and Bio-Compound Production." *Biotechnology Advances* 32, no. 8: 1535–1549.

Das, S., and V. V. Goud. 2021. "RSM-Optimised Slow Pyrolysis of Rice Husk for Bio-Oil Production and Its Upgradation." *Energy* 225: 120161.

David, E., and J. Kopac. 2018. "Pyrolysis of Rapeseed Oil Cake in a Fixed Bed Reactor to Produce Bio-Oil." *Journal of Analytical and Applied Pyrolysis* 134: 495–502.

Fernandez, E., L. Santamaria, M. Artetxe, et al. 2021. "In Line Upgrading of Biomass Fast Pyrolysis Products Using Low-Cost Catalysts." *Fuel* 296: 120682.

Gaur, S., and T. B. Reed. 2020. *Thermal Data for Natural and Synthetic Fuels*. Florida, US: CRC Press.

Ge, X., F. Xu, J. Vasco-Correa, and Y. Li. 2016. "Giant Reed: A Competitive Energy Crop in Comparison With Miscanthus." *Renewable and Sustainable Energy Reviews* 54: 350–362.

Grønli, M. G., G. Várhegyi, and C. Di Blasi. 2002. "Thermogravimetric Analysis and Devolatilization Kinetics of Wood." *Industrial & Engineering Chemistry Research* 41, no. 17: 4201–4208.

Guilhaume, N., Y. Schuurman, and C. Geantet. 2021. "The Role of Catalysis in the Valorization of Woody Biomass Fast Pyrolysis Liquids: Overview and Contribution of Ircelyon." *Catalysis Today* 373: 5–23.

Hu, X., and M. Gholizadeh. 2020. "Progress of the Applications of Bio-Oil." *Renewable and Sustainable Energy Reviews* 134: 110124.

Huang, L., Y. Chen, G. Liu, S. Li, Y. Liu, and X. Gao. 2015. "Non-Isothermal Pyrolysis Characteristics of Giant Reed (*Arundo donax* L.) Using Thermogravimetric Analysis." *Energy* 87: 31–40.

Kumar, M., S. N. Upadhyay, and P. Mishra. 2022. "Pyrolysis of Sugarcane (*Saccharum officinarum* L.) Leaves and Characterization of Products." *ACS Omega* 7, no. 32: 28052–28064.

Lee, S.-B., and O. O. Fasina. 2008. "TG-FTIR Analysis of Switchgrass Pyrolysis." Providence, Rhode Island, June 29–July 2, 2008.

Liu, S., X. Ge, Z. Liu, and Y. Li. 2016. "Effect of Harvest Date on *Arundo donax* L.(Giant Reed) Composition, Ensilage Performance, and Enzymatic Digestibility." *Bioresource Technology* 205: 97–103.

Lohitharn, N., and B. H. Shanks. 2009. "Upgrading of Bio-Oil: Effect of Light Aldehydes on Acetic Acid Removal via Esterification." *Catalysis Communications* 11, no. 2: 96–99.

Lowe, S., M. Browne, S. Boudjelas, and M. De Poorter. 2000. *100 of the World's Worst Invasive Alien Species: A Selection From the Global Invasive Species Database*. Vol. 12. Auckland: Invasive Species Specialist Group.

Martínez-Sanz, M., E. Erboz, C. Fontes, and A. López-Rubio. 2018. "Valorization of *Arundo donax* for the Production of High Performance Lignocellulosic Films." *Carbohydrate Polymers* 199: 276–285.

Monti, A., N. Di Virgilio, and G. Venturi. 2008. "Mineral Composition and Ash Content of Six Major Energy Crops." *Biomass and Bioenergy* 32, no. 3: 216–223.

Neto, C. P., A. Seca, A. Nunes, et al. 1997. "Variations in Chemical Composition and Structure of Macromolecular Components in Different Morphological Regions and Maturity Stages of *Arundo donax*." *Industrial Crops and Products* 6, no. 1: 51–58.

Nordin, A. 1994. "Chemical Elemental Characteristics of Biomass Fuels." *Biomass and Bioenergy* 6, no. 5: 339–347.

Oasmaa, A., E. Kuoppala, and D. C. Elliott. 2012. "Development of the Basis for an Analytical Protocol for Feeds and Products of Bio-Oil Hydrotreatment." *Energy & Fuels* 26, no. 4: 2454–2460.

Panwar, N. L., and A. S. Paul. 2021. "An Overview of Recent Development in Bio-Oil Upgrading and Separation Techniques." *Environmental Engineering Research* 26, no. 5: 200382.

Park, L. K.-E., S. Ren, S. Yiacoumi, X. P. Ye, A. P. Borole, and C. Tsouris. 2016. "Separation of Switchgrass Bio-Oil by Water/Organic Solvent Addition and pH Adjustment." *Energy & Fuels* 30, no. 3: 2164–2173.

Patel, A., B. Agrawal, and B. Rawal. 2020. "Pyrolysis of Biomass for Efficient Extraction of Biofuel." *Energy Sources, Part A: Recovery, Utilization, and Environmental Effects* 42, no. 13: 1649–1661.

Patel, M., and A. Kumar. 2016. "Production of Renewable Diesel Through the Hydroprocessing of Lignocellulosic Biomass-Derived Bio-Oil: A Review." *Renewable and Sustainable Energy Reviews* 58: 1293–1307.

Pawar, A., N. Panwar, and B. Salvi. 2020. "Comprehensive Review on Pyrolytic Oil Production, Upgrading and Its Utilization." *Journal of Material Cycles and Waste Management* 22: 1712–1722.

Rangel, M. d. C., F. M. Mayer, M. d. S. Carvalho, G. Saboia, and A. M. de Andrade. 2023. "Selecting Catalysts for Pyrolysis of Lignocellulosic Biomass." *Biomass* 3, no. 1: 31–63.

Saffe, A., A. Fernandez, M. Echegaray, G. Mazza, and R. Rodriguez. 2019. "Pyrolysis Kinetics of Regional Agro-Industrial Wastes Using Isoconversional Methods." *Biofuels* 10, no. 2: 245–257.

Saikia, R., R. S. Chutia, R. Kataki, and K. K. Pant. 2015. "Perennial Grass (*Arundo donax* L.) as a Feedstock for Thermo-Chemical Conversion to Energy and Materials." *Bioresource Technology* 188: 265–272.

Sluiter, A., B. Hames, R. Ruiz, et al. 2008. "Determination of Structural Carbohydrates and Lignin in Biomass." *Laboratory Analytical Procedure* 1617, no. 1: 1–16.

Sluiter, A., R. Ruiz, C. Scarlata, J. Sluiter, and D. Templeton. 2005. "Determination of Extractives in Biomass." *Laboratory Analytical Procedure* 1617, no. 4: 1–16.

Smith, R., and F. M. Slater. 2011. "Mobilization of Minerals and Moisture Loss During Senescence of the Energy Crops Miscanthus× Giganteus, Arundo Donax and *Phalaris arundinacea* in Wales, UK." *GCB Bioenergy* 3, no. 2: 148–157.

Suárez, L., M. Barczewski, P. Kosmela, M. D. Marrero, and Z. Ortega. 2023. "Giant Reed (*Arundo donax* L.) Fiber Extraction and Characterization for Its Use in Polymer Composites." *Journal of Natural Fibers* 20, no. 1: 2131687.

Temiz, A., S. Akbas, D. Panov, et al. 2013. "Chemical Composition and Efficiency of Bio-Oil Obtained From Giant Cane (*Arundo donax* L.) as a Wood Preservative." *BioResources* 8, no. 2: 2084–2098.

Van Soest, P. v., J. B. Robertson, and B. A. Lewis. 1991. "Methods for Dietary Fiber, Neutral Detergent Fiber, and Nonstarch Polysaccharides in Relation to Animal Nutrition." *Journal of Dairy Science* 74, no. 10: 3583–3597.

Yang, H., R. Yan, H. Chen, D. H. Lee, and C. Zheng. 2007. "Characteristics of Hemicellulose, Cellulose and Lignin Pyrolysis." *Fuel* 86, no. 12–13: 1781–1788.

17571707, 2024, 12, Downloaded from https://onlinelibrary.wiley.com/doi/10.1111/gcbb.70001 by South African Medical Research, Wiley Online Library on [28/11/2024]. See the Terms and Conditions (https://onlinelibrary.wiley.com/terms-and-conditions) on Wiley Online Library for rules of use; OA articles are governed by the applicable Creative Commons License